Numerical and Observational Study on Wave Conditions Near the Pilot Station

---

ABSTRACT

Pilotage services are crucial for ensuring the safe navigation of vessels entering and leaving ports. The research examines wave distributions at the pilot station using data collected from an Acoustic Doppler Current Profiler (ADCP) station and buoy. Additionally, it evaluates the impact of planned port expansions, including the construction of a new Liquefied Natural Gas (LNG) terminal and extended breakwaters, on wave characteristics and pilot operations. Numerical simulations and observational data indicate that, despite minor variations, wave height trends at the boarding area remain relatively consistent before and after expansion. The findings suggest that the proposed modifications alter wave diffraction patterns while enhancing the predictability and safety of pilot operations by reducing uncertainties in wave measurements. This study contributes to the broader understanding of marine meteorology and its implications for port safety and efficiency.

Keywords: pilotage services; wave characteristics; port expansion; pilot operation.

1. INTRODUCTION

Pilotage services are a fundamental aspect of port operations, ensuring the safe navigation of vessels during port entry and departure. Pilots utilize their in-depth knowledge of local waterways and navigational expertise to facilitate smooth port operations, including safe maneuvering and docking. However, the International Maritime Organization (IMO) does not mandate specific locations for pilot boarding, such as within or outside the breakwater. Instead, pilot boarding safety is addressed in IMO MSC.1/Circ.1428, "Pilot Transfer Arrangements – Required Boarding Arrangements for Pilots" [1], which emphasizes the need to consider wave and current effects on pilot ladders or gangways during boarding in open waters. Ideally, pilot transfers should occur in calm, sheltered areas within the breakwater. Additional precautions must be implemented if boarding occurs in exposed waters to protect both pilots and vessels. Although IMO MSC.1/Circ.1428 does not prescribe exact boarding locations, its safety guidelines have led port authorities worldwide to establish operational procedures to enhance pilot safety and efficiency. For example, the United States Coast Guard (USCG) [2] recommends pilot boarding areas, prioritizing locations within breakwaters or other stable waters to minimize risks, particularly under adverse weather conditions. Similarly, the UK's Maritime and Coastguard Agency (MCA) [3] advises that pilot boarding should, whenever possible, be conducted within protected areas to reduce wave impact and vessel movement, thereby improving safety. The Maritime and Port Bureau (MOTC) [4] requires pilot boarding in stable and secure waters in Taiwan. However, Taiwan's distinct marine meteorological conditions prevent a standardized requirement for boarding within breakwaters. As a result, most pilot transfers occur in open waters outside the port, where wave conditions can significantly influence the safety and efficiency of pilot operations.

Multiple factors influence pilot boarding safety, including human elements, vessel characteristics, channel conditions, sea states, and weather patterns. As an applied field, marine transportation relies heavily on accurate meteorological data to ensure safe vessel navigation during port entry and exit. With continuous changes in port water environments, it is essential to evaluate external influences comprehensively and formulate effective strategies to address complex navigational challenges [5-14]. Beyond ensuring vessel safety, pilots are also responsible for safeguarding port infrastructure, improving operational efficiency, and adhering to maritime regulations and insurance requirements. However, unfavorable vessel heading or speed can increase the likelihood of accidents. Wave dynamics play a key role in determining the safety and predictability of pilot transfers. The irregularity and variability of waves create additional challenges, increasing risks for vessels and boarding personnel. For instance, significant wave height fluctuations can cause vertical vessel movements, affecting boarding stability. Wave period variations introduce unpredictable ship motions, making transfers more challenging. Furthermore, wave direction influences vessel behavior—side waves induce rolling, while waves from the bow or stern lead to pitching, which can compromise pilot boarding safety. As a result, pilots and crew must continuously monitor and respond to wave conditions to ensure a secure boarding process. Wave formation is closely tied to wind characteristics. For example, [15] examined the quantitative relationship between wave height, wind speed, and fetch, concluding that height is proportional to the square of wind speed in fully developed waves. Conversely, [16] suggested a direct proportionality between wave height and wind speed. Large-scale research projects, such as the European Union's 1998 initiative "Waves and Storms in the North Atlantic" (WASA) [17], primarily rely on numerical modeling to predict long-term wave trends and analyze their distribution. Subsequent studies have incorporated remote sensing and long-term observational data for statistical analysis [18-24]. While much research has focused on human factors [25], there is comparatively less emphasis on the interactions between maritime traffic and environmental conditions, mainly because human-related variables are more straightforward to analyze and control. Ports are fundamental centers for marine engineering advancements and crucial nodes in land-sea transportation networks. The success of port infrastructure depends on ensuring vessels' safe entry, navigation, mooring, and cargo operations. As ships continue to increase, pilots' challenges have become more complex. Given the demands of their profession, pilots must often board vessels using rope ladders, regardless of weather conditions. This exposes them to risks such as falling into the water or being caught between vessels in rough seas. Balancing safety and efficiency is a critical aspect of pilotage, requiring exceptional navigational expertise and prompt decision-making to maintain smooth port operations while minimizing accident risks. Since vessel maneuvering is influenced by human factors, ship characteristics, and environmental conditions, pilots must continuously process and manage vast amounts of information to regulate vessel movement and achieve safe navigation [26-29]. During port entry and departure, vessels are subject to various external forces, including wind and currents, which can significantly affect speed and course stability. Additionally, wave conditions are crucial in maritime safety, particularly at narrow port entrances where wave height variations can directly impact vessel stability. Ensuring safe pilot boarding requires a thorough understanding of tidal currents, wave patterns near the port, and the influence of local bathymetry on nearshore hydrodynamics. Pilots can make informed decisions to enhance safety and operational efficiency by accurately assessing these factors.

The Taiwan Strait is a crucial global shipping passage. Its distinct geographical position makes the region’s marine meteorological conditions highly susceptible to monsoonal influences and topographical effects, leading to substantial and steady winds in the central part of the strait. The primary ports in this region include Taichung Port and Mailiao Port. Taichung Port consists of commercial, industrial, and fishing sections, whereas Mailiao Port mainly serves industrial purposes. Both are artificial harbors fortified by breakwaters and sea dikes. Seasonal monsoons dominate the Taiwan Strait, with northeast monsoons prevailing in winter and southwest monsoons in summer. Due to planetary wind systems and the region’s topography, the northeast monsoon tends to be more intense. To minimize its impact on vessels, Mailiao Port’s entrance is aligned southwest (SW), helping to mitigate the influence of wind-driven waves and ensuring safer navigation. Taichung Port shares similar marine meteorological conditions, but its entrance faces west-northwest (WNW), with breakwaters positioned nearly perpendicular to the shoreline. This structural design reduces the effects of northeast monsoons and wind-induced waves on vessel operations. Breakwaters are critical protective structures that shield the harbor from incoming waves and maintain stable water conditions for docking activities. However, their placement alters fluid dynamics, potentially shifting water flow patterns and redistributing energy within the harbor. The Taiwan Strait is also heavily influenced by tidal currents, with the predominant water movement following a northeast-to-southwest (NE-SW) direction. In addition to wind-driven waves at Taichung Port, vessels must contend with cross-currents, increasing navigational risks when entering or exiting the harbor.

In recent years, the expansion of offshore wind energy has contributed to increased maritime activity at Taichung Port. As an "inner-excavated" port, its navigation channels and harbor waters have been created through excavation, with external breakwaters and sea dikes providing protection. However, in confined port areas, the interaction between waves and tidal currents can create complex hydrodynamic conditions, raising the risks associated with vessel maneuvering. To support Taiwan's energy transition—shifting towards more significant natural gas usage while reducing coal dependency—Taichung Port has plans to build a new liquefied natural gas (LNG) terminal (the fifth terminal). It may extend its breakwaters by over 5 kilometers. Modifications to the layout of the external breakwaters could influence wave-current interactions, potentially affecting hydrodynamic stability and the predictability of pilot boarding operations. This study examines Taichung Port as a case study, aiming to help pilots accurately assess wave conditions and enhance navigational safety through refined piloting strategies and timely decision-making. Marine meteorological data will be analyzed to characterize environmental conditions, while numerical simulations will be used to evaluate wave-current interaction trends. Field measurements will serve as a reference for validating numerical models, allowing for an in-depth investigation of hydrodynamic distribution near the pilot station before and after port expansion. The findings will provide crucial insights to support pilots in conducting safe and efficient vessel operations under varying marine meteorological conditions, improving overall port safety and operational efficiency.

2. MARINE METEOROLOGICAL DATA ANALYSIS

2.1 Port background

Taichung Port is situated in the central region of the Taiwan Strait and is equipped with modern docking and repair facilities that offer vessel maintenance, servicing, and technical support. Figure 1 provides an overview of relevant details about the port. The pilot station is roughly 0.6 nautical miles west of the southern breakwater, near the junction of the outer harbor channel, with coordinates 24°17'27.7"N, 120°29'22.4"E, and a bearing of 274°. Vessels arriving at the port navigate through the southern approach of the separation zone on a course of 065° toward the pilot station before adjusting to 114° to enter the harbor. Departing ships follow the main channel, passing the southern breakwater on a 294° heading, and upon exiting the separation zone, they may alter course either northward (N) or southwest (SW). Furthermore, Taichung Port has expansion plans, as shown by the red line in Figure 1, which includes extending the outer breakwater by more than 5 kilometers to accommodate the construction of the new LNG terminal (the fifth terminal). Modifying the breakwater structure may influence hydrodynamic conditions by altering wave-current interactions, which could affect the stability and predictability of pilot boarding operations.
Vessel movements in the water area between the outer harbor channel and the breakwater are primarily affected by environmental conditions such as tides, waves, currents, and wind. Evaluating the safety of port entry requires consideration of multiple factors, including ship maneuverability, external environmental forces, and harbor characteristics. This study used data from monitoring stations near Taichung Port to analyze these influences. As illustrated in Figure 1, the "Wind" (24°17'59"N, 120°29'12"E) and "ADCP" (24°18'02"N, 120°29'05"E) stations were established by the Transportation Technology Research, I.O.T, M.O.T.C., while the "Tide" (24°17'15"N, 120°31'53"E) and "Data buoy" (24°14'15"N, 120°24'32"E) stations were deployed by the Central Weather Administration.

Fig. 1 Layout and marine meteorological station locations in Taichung Port

2.2 Wind force condition

This study gathered wind data from the measurement station at coordinates 24°17'59" N and 120°29'12" E, as depicted in Figure 2. The observation period covers January 1, 2009, to December 31, 2024, with an overall data collection rate of 94.3%. Wind measurements were recorded every 10 minutes and analyzed on an hourly basis. However, the 1-minute average wind speed is a more relevant reference for port and vessel operations, typically measuring around 1.15 times the 10-minute average wind speed [30]. Accordingly, the wind data in this study will be adjusted using this conversion factor.

Port entry and exit regulations, as specified in the Taichung Port Vessel Traffic Service Guide by the Taichung Port Branch [31], state that when the recorded average wind speed reaches 20 m/s or forecasts indicate a continued increase, port entry operations may be suspended. According to the Regulations for the Entry, Exit, and Berthing Operations of LNG Ships at Taichung Port [32], LNG vessels are subject to stricter wind limitations, with port entry being suspended when the average wind speed exceeds 15 m/s. Additionally, the Wind Control Standards for Entry and Exit at Taichung Port: Taichung Port Traffic Service Guide by the Central Navigation Affairs Center, Maritime and Port Bureau, Ministry of Transportation and Communications [33] concludes that guided entry may still be permitted under specific conditions when wind speeds range from 20 to 22 m/s. However, port entry operations will be halted if the average wind speed surpasses 22 m/s. This study utilizes quadrative deviation as a dispersion indicator to analyze the distribution of wind force at different levels and assess statistical probabilities. Wind force data undergo outlier analysis to detect anomalous observations, and cumulative probabilities for the 75%, 50%, and 25% percentiles are computed. A summary of the analysis results is provided in Table 1 to Table 3.

Table 1. Main wind speed and direction in Taichung Port

Season	Wind speed	Wind direction
Spring	0~5 m/s (31.9 %)	NNE (31.3 %)
Summer	0~5 m/s (37.2 %)	SSW (21.5 %)
Autumn	0~5 m/s (31.9 %)	NNE (47.5 %)
Winter	5~10 m/s (18.9 %)	NNE (45.7 %)
Year	0~5 m/s (28.4%)	NNE (34.8%)

**Data collection and analysis period: 2009-2024*

Table 2. Wind speeds greater than 15 and 20 m/s in Taichung Port

Season	Over 15 m/s	Over 20 m/s
Spring	16.5 %	6.3 %
Summer	4.6 %	1.2 %
Autumn	33.2 %	16.0 %
Winter	36.2 %	19.0 %
Year	24.1 %	11.6 %

**Data collection and analysis period: 2009-2024*

Table 3. Cumulative probabilities of wind speed in Taichung Port

Season	25%	50%	75%
Spring	3.9 m/s	7.5 m/s	12.4 m/s
Summer	3.3 m/s	6.3 m/s	9.7 m/s
Autumn	4.5 m/s	10.2 m/s	17.5 m/s
Winter	6.3 m/s	12.5 m/s	19.1 m/s
Year	4.1 m/s	8.5 m/s	15.2 m/s

**Data collection and analysis period: 2009-2024*

2.3 Wave characteristics

The wave data used in this study were collected from January 1, 2009, to December 31, 2024, with an overall data collection rate of approximately 80.0%. The analysis follows the guidelines outlined in the Regulations for the Entry, Exit, and Berthing Operations of LNG Ships at Taichung Port [32], which state that operations must be suspended if the significant wave height within the northern breakwater's sheltered area exceeds 2.5 meters. The methodology for analyzing wave data mirrors the statistical approach applied to wind data, where cumulative probabilities for the 75%, 50%, and 25% percentiles are computed. A summary of the analysis results is presented in Table 4 to Table 7.

Table 4. Main wave parameters in Taichung Port

Season	Wave height	Wave direction	Wave period
Spring	1~2 m (30.0 %)	NNE (34.3 %)	6~7 s (21.6 %)

Summer	0~1 m (51.4 %)	W (23.8 %)	6~7 s (18.4 %)
Autumn	1~2 m (34.1 %)	NNE (53.5 %)	6~7 s (28.2 %)
Winter	2~3 m (27.3 %)	NNE (42.0 %)	7~8 s (23.5 %)
Year	1~2 m (29.7 %)	NNE (36.4 %)	7~8 s (21.6 %)

**Data collection and analysis period: 2009-2024*

Table 5. Wave height greater than 2.5m in Taichung Port

Season	Over 2.5m
Spring	7.3%
Summer	2.2%
Autumn	25.4%
Winter	24.6%
Year	16.3%

**Data collection and analysis period: 2009-2024*

Table 6. Cumulative probabilities of wave height in Taichung Port

Season	25%	50%	75%
Spring	0.61 m	1.02 m	1.63 m
Summer	0.52 m	0.69 m	0.93 m
Autumn	1.08 m	1.72 m	2.35 m
Winter	0.95 m	1.78 m	2.44 m
Year	0.69 m	1.22 m	2.07 m

**Data collection and analysis period: 2009-2024*

Table 7. Cumulative probabilities of wave period in Taichung Port

Season	25%	50%	75%
Spring	5.0 s	6.0 s	7.0 s
Summer	4.0 s	5.5 s	6.8 s
Autumn	6.0 s	7.0 s	7.8 s
Winter	6.0 s	7.0 s	7.7 s
Year	5.3 s	6.4 s	7.3 s

**Data collection and analysis period: 2009-2024*

3. MODEL SETUP AND VERIFICATION

3.1 Wave model setup

In actual operations, large vessels often create a sheltered zone by positioning themselves to block wind and waves, enhancing the safety of pilot boarding. However, as waves travel from offshore to nearshore regions, their energy transforms due to various wave deformation processes, including shoaling, refraction, diffraction, and breaking, resulting from coastal water depth variations. Additionally, wave energy is dissipated through mechanisms such as wave breaking and bottom friction. This study applies computational methods to analyze the energy changes of waves as they propagate from deep water to coastal areas [34].

$$\frac{D^2\varphi}{Dt^2}+\left(\nabla\cdot\vec{U}\right)\frac{D\varphi}{Dt}-\nabla\cdot\left(CC_g\nabla\varphi\right)+\left(\sigma^2-k^2CC_g\right)\varphi=0 \tag{1}$$

Assuming non-rotational, single-frequency linear surface waves, the wave potential function can be represented as follows:

$$\varphi\left(\vec{x},\vec{y},z,t\right)=f\left(z,h\right)\varphi\left(\vec{x},\vec{y},t\right) \tag{2}$$

Here $f(z,h)=\cosh[k(h+z)]/\cos kh$, where k represents the wave number, h denotes the water depth, z is the vertical position, and t corresponds to time. Under the assumption of single-period harmonic wave motion, the wave potential function can be reformulated as follows:

$$\varphi\left(\vec{x},\vec{y},t\right)=\mathrm{Re}\left\{ae^{is}e^{i\omega t}\right\} \tag{3}$$

To solve this problem, substitute the potential energy function in Equation (3) into Equation (1) and then discuss the real and imaginary parts separately:

$$\frac{1}{aCC_g}\left\{\left(\vec{U}\cdot\nabla a\right)\left[\left(\vec{U}\cdot\nabla\right)+\left(\nabla\cdot\vec{U}\right)\right]\right\}-\frac{1}{a}\left[\nabla^2 a+\frac{1}{CC_g}\left(\nabla CC_g\cdot\nabla a\right)\right]-k^2+\left|\nabla s\right|^2=0 \tag{4}$$

$$\nabla\cdot\left[a^2\sigma\left(U+C_g\right)\right]=0 \tag{5}$$

Equations (4) and (5) are the equations of motion of the wave under the influence of wave-current interaction before it breaks. When the flow velocity $\vec{U}$ is known, solving this system of linear parabolic equations can simultaneously yield the amplitude function $a(x,y)$ and the wave number $\left|\nabla s\right|$. When $\vec{U}=0$, Equations (4) and (5) become:

$$\frac{1}{a}\left\{\frac{\partial^2 a}{\partial x^2}+\frac{\partial^2 a}{\partial y^2}+\frac{1}{cc_g}\left[\nabla a\cdot\nabla\left(cc_g\right)\right]\right\}+k^2-\left|\nabla s\right|^2=0 \tag{6}$$

$$\nabla\cdot\left[a^2CC_g\nabla s\right]=0 \tag{7}$$

In addition, the energy representation in the wave-breaking zone in Equation (5) must be corrected due to energy dissipation. According to the energy flux principle, ignoring the bed friction effect, the following expression is used [35]:

$$\begin{aligned}
&\frac{d\left(EC_g\right)}{dx}=-\varepsilon\\
&\varepsilon=\frac{1}{2}\rho V_e\left(kH_B\right)^2\\
&V_e=V_{eB}\left(\frac{\frac{H_B}{2}-c'h_B}{\gamma' h_B}\right)\\
&V_{eB}=\frac{5S_Bg}{8k_B\rho}\frac{1}{\sqrt{1-C_0}}\\
&S_B=\frac{\tan\beta}{1+\frac{3r^2}{2}}
\end{aligned} \tag{8}$$

Where *c*’ is the wave amplitude to water depth ratio in the recovery zone, in wave-current interaction, the energy dissipation caused by the nearshore current in the wave-breaking zone is minimal and can be ignored. Therefore, according to the energy amplitude representation in Equation (8), it can be expressed as follows:

$$\nabla\cdot\left[\frac{E}{\sigma}\left(\vec{U}+C_g\right)\right]=-\frac{5}{16}\frac{\rho g^2k_B}{\sigma^2}\frac{\tan\beta}{1+\frac{3r'^2}{2}}\frac{1}{\sqrt{1-C_0}}\sqrt{\frac{\frac{H_B}{2}-c'h_B}{r'h_B}}\left(H_B\right)^2 \tag{9}$$

Combined with the energy expression in the wave-breaking zone in Equation (6), Equation (9) is modified as follows:

$$\begin{aligned}
&\nabla\cdot\left[a^2\sigma\left(\vec{U}+C_g\right)\right]=\nabla\cdot\left[\frac{2g}{\rho}\frac{E}{\sigma}\left(\vec{U}+C_g\right)\right]=\\
&\quad-\frac{5}{8}\frac{g^2k_B}{\sigma}\frac{\tan\beta}{1+\frac{3r'^2}{2}}\frac{1}{\sqrt{1-\frac{c'}{r'}}}\sqrt{\frac{\frac{H_B}{2}-c'h_B}{r'h_B}}\left(H_B\right)^2
\end{aligned} \tag{10}$$

In Equations (8) to (10), the subscript B represents the value of the wave-breaking zone. Since the phase function of ϕ is $x\left(\vec{x},t\right)=s\left(\vec{x}\right)-\omega t$, the wave number obtained from the modified gentle slope wave equation can be expressed as:

$$\vec{k}=\nabla x=\nabla s \tag{11}$$

Since the wave number is a vector, to obtain $\left|\nabla s\right|$ according to Equations (4), (5), or (10), the direction angle of the wave must be known. Solving for *a*, $\left|\nabla s\right|$, and θ involves only two insufficient equations. Apply the assumption of the irrotational gradient of wave phase function in linear wave theory:

$$\begin{aligned}&\nabla\times\left(\nabla s\right)=0\\&\nabla s=\left|\nabla s\right|\cos\theta\vec{i}+\left|\nabla s\right|\sin\theta\vec{j}\\&\frac{\partial}{\partial x}\left(\left|\nabla s\right|\sin\theta\right)-\frac{\partial}{\partial y}\left(\left|\nabla s\right|\cos\theta\right)=0\end{aligned} \tag{12}$$

Among them, Equations (4), (5), (10), and (12) are the governing equations for wave pattern calculation. Outside the surf zone, finite difference calculations are performed using Equations (4), (5), and (12); inside the surf zone, finite difference calculations are performed using Equations (4), (10), and (12).

3.2 Modeling procedure and validation

The model calculation area in this study, as depicted in Figure 2, is centered on Taichung Port and covers a rectangular region measuring 10.8 km along the coastline and 20.0 km offshore. Figure 2(a) presents the existing port configuration, whereas Figure 2(b) illustrates the layout after expansion. The overall numerical topography setup and input parameters are provided in Table 8. A comparison between the simulated wave field results and the field ADCP observation data is displayed in Figure 3. The findings demonstrate that the computed wave height, period, and direction closely align with the observed data.

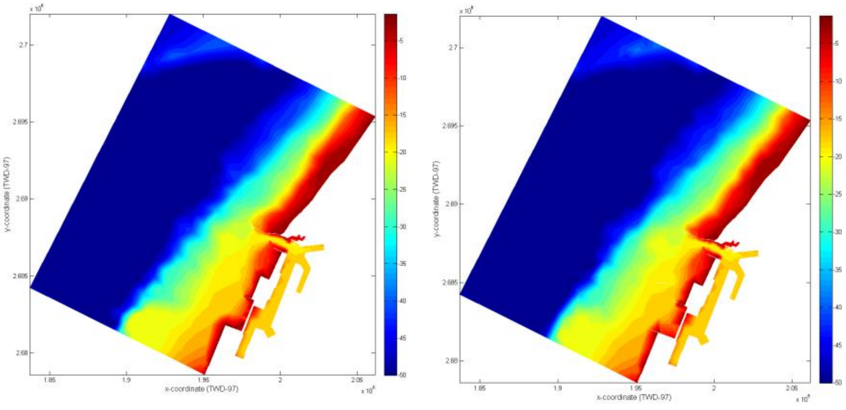

(a) Current Port Configuration (b) Expanded Port Configuration

Fig. 2 Numerical topography used for model calculations

Table 7. Cumulative probabilities of wave period in Taichung Port

Particulars	**Value**
Calculation Area	10.8 * 21.0 km
Spatial Grid	30 * 30 m
Number of Grids	360 * 700
Rotation Angle	25°
Coordinate Origin (TWD 97)	195062.513, 2678561.060
Temporal Grid	1.5 sec
Time Scale	1.0

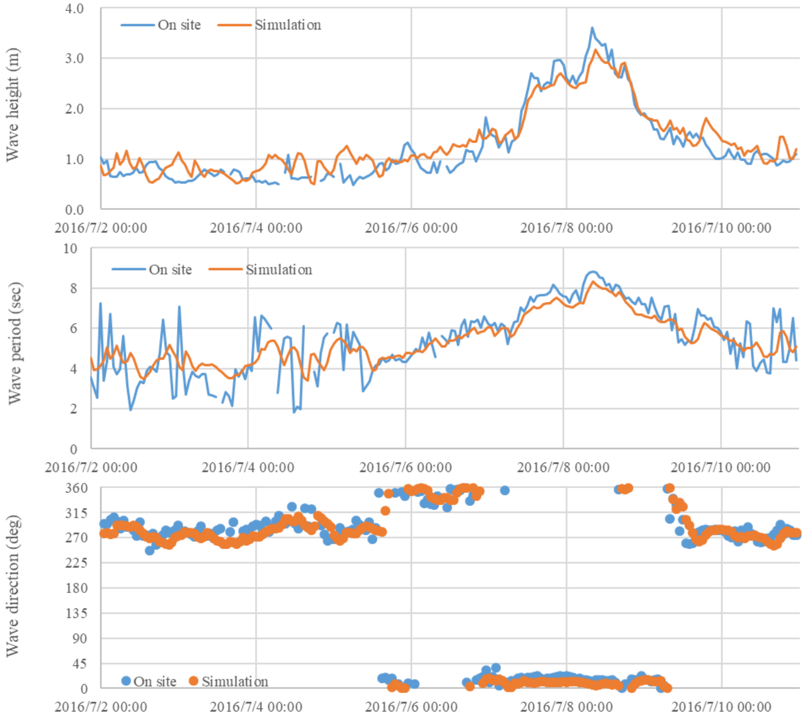

Fig. 3 Comparison of numerical model results with measured wave data

In addition, to more effectively evaluate whether the model accurately represents the calculation results, model validation should be based on quantitative analysis as much as possible. This study uses a quantitative analysis of the degree of agreement and deviation between simulated data and measured data to verify the model in environmental science, oceanography, hydrology, etc. Specifically, the study used the Agreement coefficient and Averaged deviation to evaluate the degree of difference between the measured data and the simulated data [36], which are defined as follows:

$$D = 1 - \frac{\sum_{n=1}^{N}\left(P_n - O_n\right)^2}{\sum_{n=1}^{N}\left(\left|P_n - O\right| + \left|O_n - O\right|\right)^2} \tag{13}$$

$$P = \frac{\sum_{n=1}^{N}\left(P_n - O_n\right)}{\sum_{n=1}^{N} O_n} \tag{14}$$

Where P_n represents the calculated value, O_n and O represent the measured value and its average value, respectively; D=1 means complete agreement, and P=0 means no deviation. The study calculated the Agreement Coefficient (D) and Averaged Deviation (P), and the results are summarized in Table 8. When the Agreement Coefficient (D) is more significant than 0.7, the model's fit is considered to be of reference value; when it is more significant than 0.85, it is highly consistent; and when it is less than 0.5, it may be necessary to adjust the model parameters or retest the data. As for Averaged Deviation (P), the closer the value is to 0, the smaller the average error between the simulation and measured data is. When the average deviation is less than 0.05, the systematic error of the model can be ignored. When the average deviation is more significant than 0.2, there may be obvious overestimation or underestimation, which requires further analysis.

For wave height, D = 0.96 and P = 0.07; for wave period, D = 0.87 and P = -0.01; and for wave direction, D = 0.85 and P = 0.0%. Overall, the results show reasonable agreement with the field measurements, indicating that the model effectively reproduces the wave distribution characteristics near Taichung Harbor.

Table 8. Quantitative comparison of measured data and simulation results

Parameter	Agreement Coefficient (D)	Averaged Deviation (P)
Wave height	0.96	0.07
Wave period	0.87	-0.01
Wave direction	0.85	0.01

4. MODEL APPLICATION

4.1 Analysis Conditions

According to the vessel entry restrictions for Taichung Port outlined in the Taichung Port Vessel Traffic Service Guide issued by the Taichung Port Branch, vessel entry operations must be suspended when the recorded average wind speed reaches 20 m/s or if forecasts predict a continuous increase in wind speed. Additionally, the Wind Control Standards for Entry and Exit at Taichung Port established by the Central Navigation Affairs Center, Maritime and Port Bureau, Ministry of Transportation and Communications, allow vessel guidance into the port when the average wind speed is between 20 and 22 m/s; however, entry operations are suspended if the wind speed exceeds 22 m/s. Furthermore, the Regulations for the Entry, Exit, and Berthing Operations of LNG Ships at Taichung Port specify that LNG ship operations must be halted when the average wind speed surpasses 15 m/s or when the indicative wave height in the north breakwater shelter area exceeds 2.5 m. A cumulative probability analysis of wind and wave data from the previous section is summarized in Table 9 to 10. Under the 75% cumulative probability condition during the fall and winter seasons, wind speeds exceed the thresholds stated in the LNG ship operation regulations. However, wave heights generally remain within the prescribed limits, with only the winter season's 75% cumulative probability condition approaching the 2.5 m wave height threshold.

At Taichung Port, the ADCP (24°18'02" N, 120°29'05" E) is located 150 meters beyond the tip of the North Breakwater at a depth of 25 meters, as illustrated in

Figure 1. Due to the potential shielding effect of the breakwater, wave data recorded at this site may not fully reflect the wave conditions at the pilot boarding location. Additionally, Taichung Port is planning the construction of a new LNG receiving station (Fifth Receiving Station), marked by the red line in Figure 4. This project includes extending the outer breakwater by more than 5 kilometers. Such modifications to the outer breakwater structure could influence water dynamics through wave-current interactions, potentially affecting the accuracy of wave predictions and the safety of pilot boarding operations. In the following analysis, this study will simulate wave distribution patterns before and after the expansion under different cumulative probability conditions for each season, as detailed in Table 9 to 10, and evaluate the results accordingly.

Table 9. Modeled calculation input wind conditions

Season	25%	50%	75%	Dir.
Spring	3.9 m/s	7.5 m/s	12.4 m/s	NNE
Summer	3.3 m/s	6.3 m/s	9.7 m/s	SSW
Autumn	4.5 m/s	10.2 m/s	17.5 m/s	NNE
Winter	6.3 m/s	12.5 m/s	19.1 m/s	NNE

Table 10. Modeled calculation input wave conditions

Season	25%	50%	75%	Dir.
Spring	0.61 m/ 5.0 s	1.02 m/ 6.0 s	1.63 m/ 7.0 s	NNE
Summer	0.52 m/ 4.0 s	0.69 m/ 5.5 s	0.93 m/ 6.8 s	W
Autumn	1.08 m/ 6.0 s	1.72 m/ 7.0 s	2.35 m/ 7.8 s	NNE
Winter	0.95 m/ 6.0 s	1.78 m/ 7.0 s	2.44 m/ 7.7 s	NNE

4.2 Model Calculation Results

Calculations were conducted based on the cumulative probability conditions of wind and wave parameters for each season, along with their predominant directions, and the results are illustrated in Figures 4 to 7. As observed in these figures, except for summer—where the predominant wave direction (W) and wind direction (SSW) differ from other seasons—the prevailing wind and wave directions in spring, autumn, and winter are consistently NNE. With the modified outer breakwater configuration at the LNG receiving station (Fifth Receiving Station), the shielding effect of the North Breakwater significantly reduces the impact of wave diffraction within the port. However, since the entrance to Taichung Port is approximately WNW, and the predominant wave direction in summer is W, there is no substantial decrease in wave height distribution near the pilot boarding area. Furthermore, the Regulations for the Entry, Exit, and Berthing Operations of LNG Ships at Taichung Port primarily rely on wave data from the measurement station (24°18'02" N, 120°29'05" E) located within the sheltered zone of the North Breakwater. To accommodate increasing maritime traffic and mitigate the risks associated with relying on a single station for port operation safety assessments, the Central Weather Administration established a new buoy station (Code C6F01) in 2019. This station, positioned offshore at a depth of approximately 18.5 meters, is located at 24°14'15" N, 120°24'32" E, as depicted in Figure 1.

This study compares data from the ADCP and Buoy stations with conditions at the boarding point (24°17'26" N, 120°29'22" E). Figures 8 and 9 present the simulation results under current conditions. In Figure 8, when the predominant wind and wave directions are NNE, the wave height at the boarding point is approximately 0.38 times the ADCP wave height minus 0.25 or 0.37 times the Buoy wave height minus 0.23, as expressed in Equation (15). In Figure 9, for summer conditions where the predominant wave direction is W, and the predominant wind direction is SSW, the wave height near the boarding point is approximately 0.97 times the ADCP wave height or 1.07 times the Buoy wave height minus 0.12, as indicated in Equation (16). Figures 10 and 11 illustrate the simulation results following the port expansion. In Figure 10, under conditions where both the primary wind and wave directions remain NNE, the wave height at the boarding point is approximately 0.39 times the ADCP wave height minus 0.23 or 0.37 times the Buoy wave height minus 0.21, as described in Equation (17). Meanwhile, in Figure 11, for summer conditions with a primary wave direction of W and a primary wind direction of SSW, the wave height near the boarding point is approximately 0.98 times the ADCP wave height minus 0.01 or 1.09 times the Buoy wave height minus 0.14, as stated in Equation (18). This study evaluates wave height variations at the boarding point by comparing data from the ADCP wave measurement station and the Taichung buoy (Buoy).

The findings indicate that while the overall trend in wave height variations remains similar under current and post-expansion conditions, there are slight differences in the actual values. These simulation results help address challenges associated with data gaps from a single measurement station, offering more reliable predictions and safety evaluations for boarding operations.

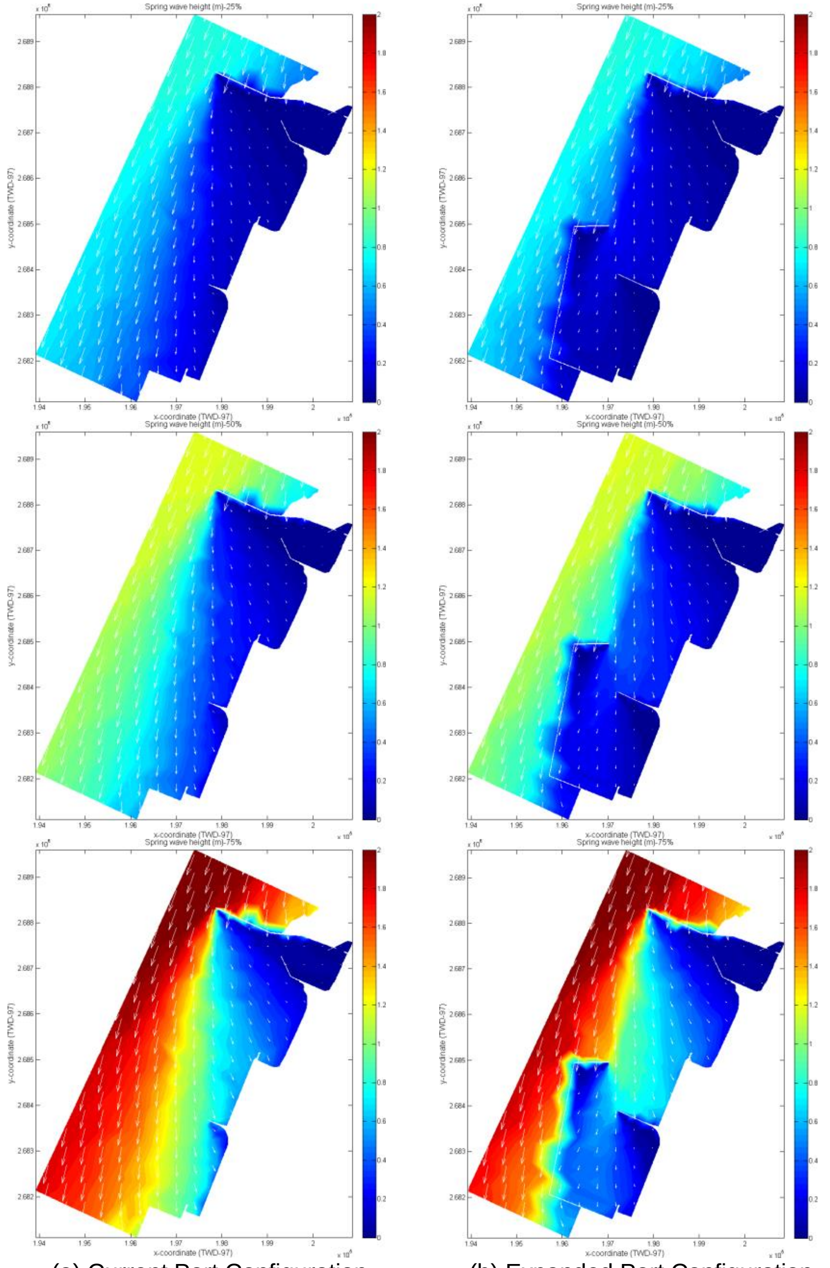

(a) Current Port Configuration (b) Expanded Port Configuration

Fig. 4 Wave Distribution Under Different Probability Conditions in Spring

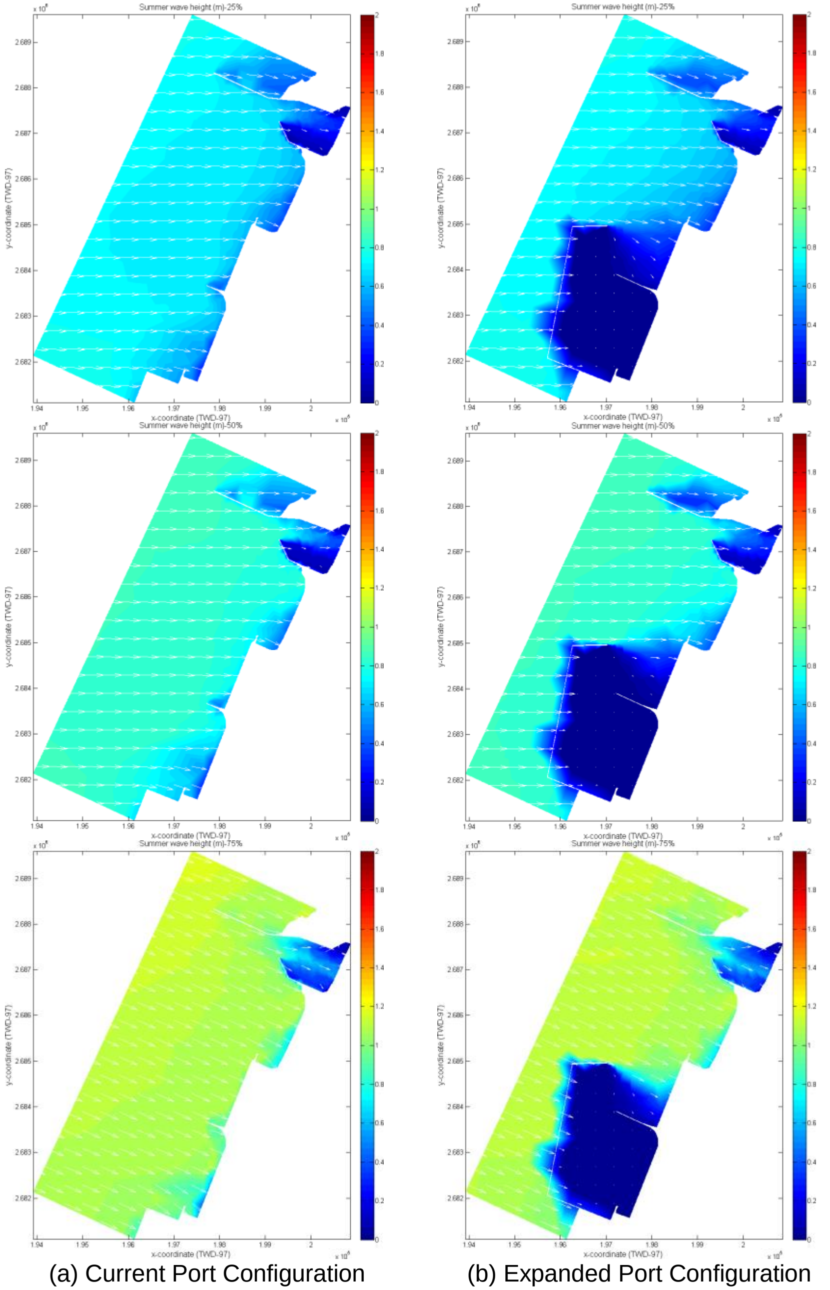

(a) Current Port Configuration (b) Expanded Port Configuration

Fig. 5 Wave Distribution Under Different Probability Conditions in Summer

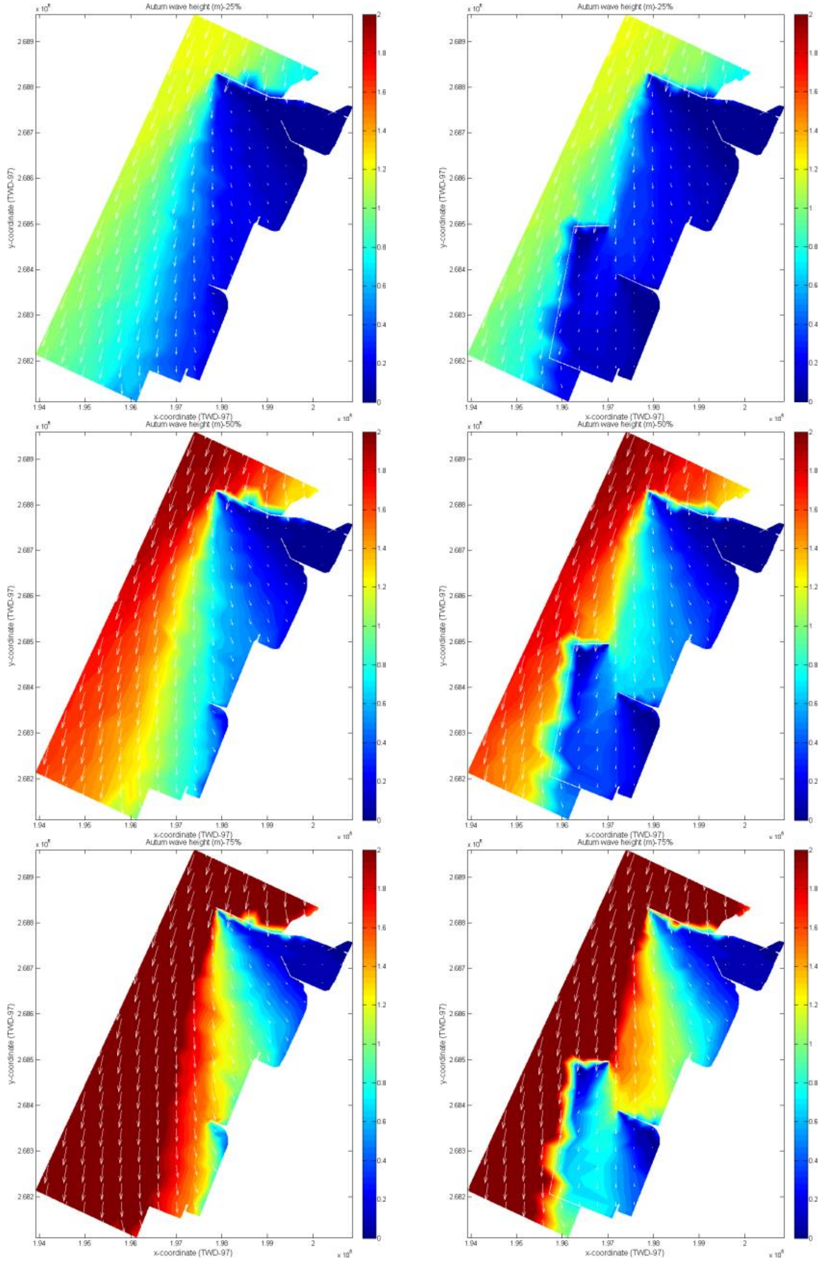

(a) Current Port Configuration (b) Expanded Port Configuration

Fig. 6 Wave Distribution Under Different Probability Conditions in Autumn

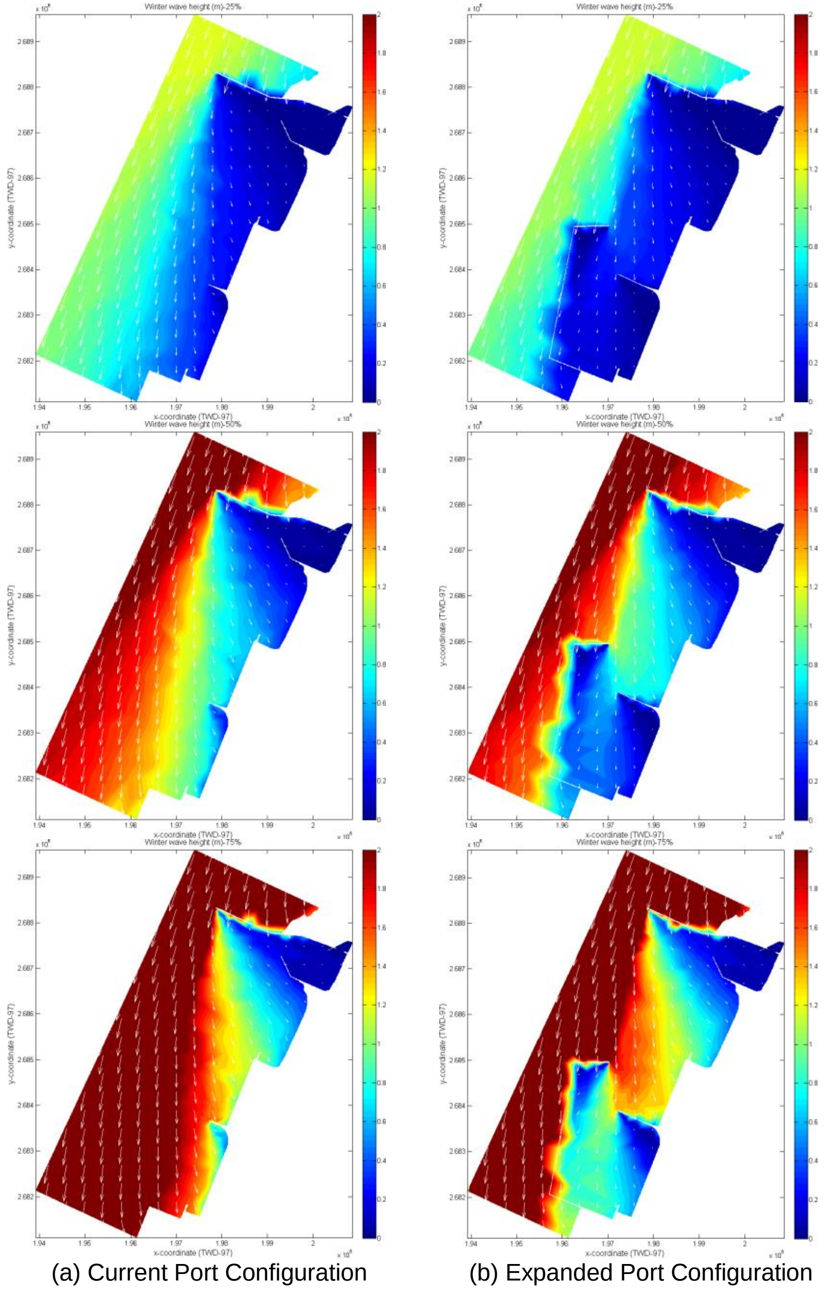

(a) Current Port Configuration (b) Expanded Port Configuration

Fig. 7 Wave Distribution Under Different Probability Conditions in Winter

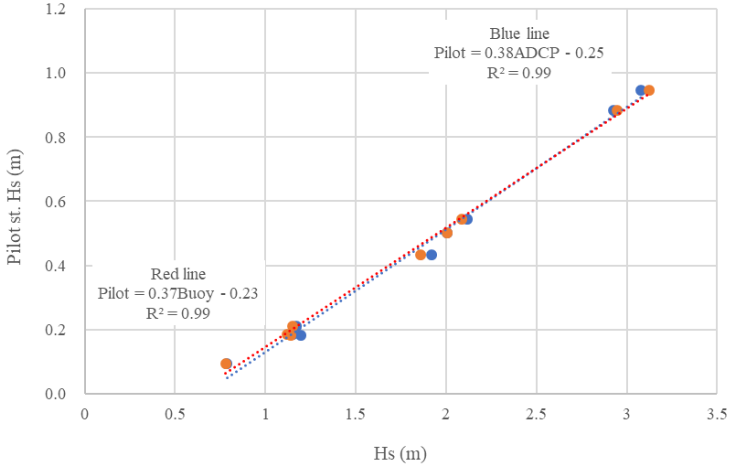

Fig. 8 Wave height distributions for non-summer conditions.

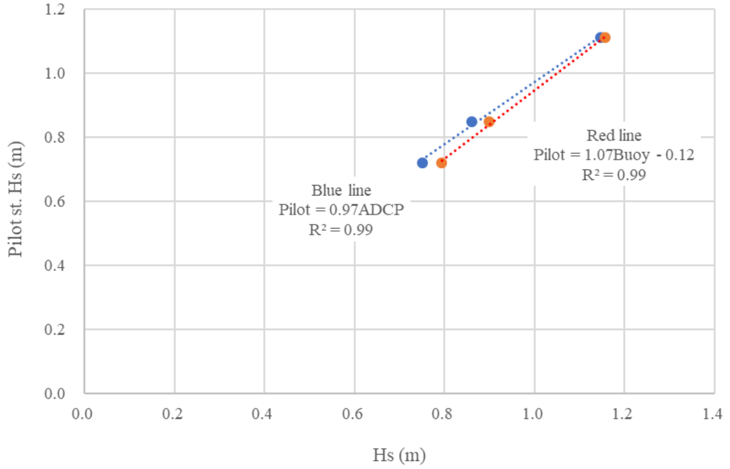

Fig. 9 Wave height distributions for summer conditions.

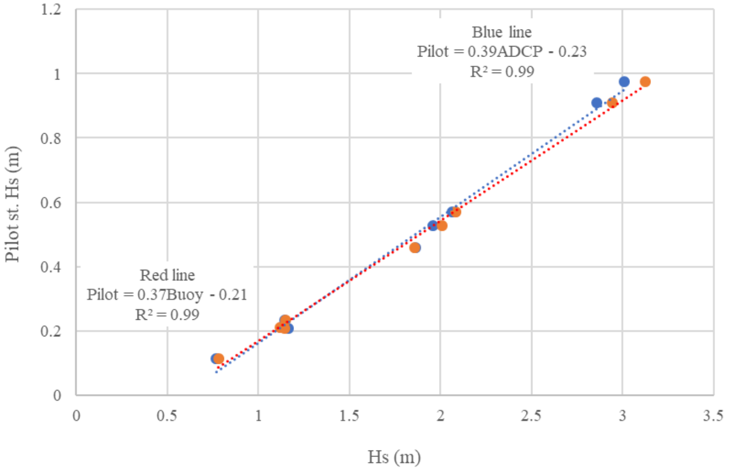

Fig. 10 Wave height distribution for non-summer conditions after expansion.

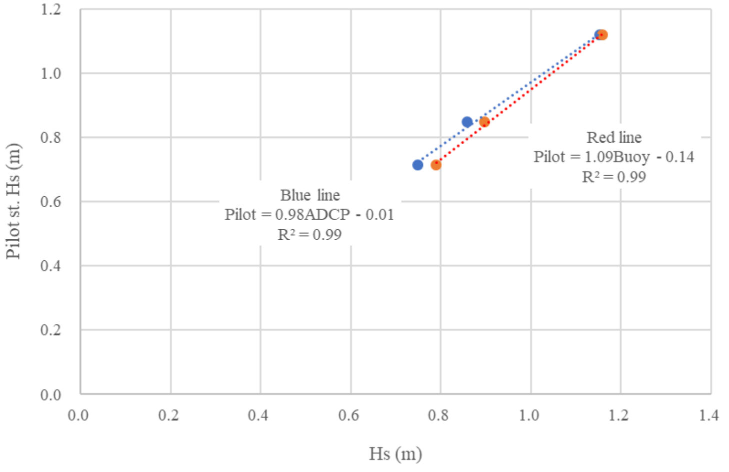

Fig. 11 Wave height distribution for summer conditions after expansion.

Non-Summer Wind and Wave Conditions:

$$Pilot = 0.38 \cdot ADCP - 0.25 = 0.37 \cdot Buoy - 0.23 \tag{15}$$

Summer Wind and Wave Conditions:

$$Pilot = 0.97 \cdot ADCP = 1.07 \cdot Buoy - 0.12 \tag{16}$$

Non-Summer Wind and Wave Conditions After Expansion:

$$Pilot = 0.39 \cdot ADCP - 0.23 = 0.37 \cdot Buoy - 0.21 \tag{17}$$

Summer Wind and Wave Conditions After Expansion:

$$Pilot = 0.98 \cdot ADCP - 0.01 = 1.09 \cdot Buoy - 0.14 \tag{18}$$

4. CONCLUSION

Pilots rely on their expertise in navigation and in-depth knowledge of local waters to maintain the smooth operation of the port. However, waves' unpredictable nature and variability can make boarding operations challenging and hazardous. This study examines wave height distribution based on data from the bottom-mounted wave and current station located north of the Taichung Port breakwater and from the Taichung buoy situated southwest of the port relative to the boarding point. This methodology helps mitigate uncertainties caused by missing data from individual measurement stations and enhances the practicality of real-world operations. The findings of this study lead to the following conclusions:

Influence of Irregular Wave Patterns: The unpredictability and variability of waves introduce challenges and potential risks to boarding operations. This study enhances the understanding of wave conditions by analyzing wave height distributions from multiple measurement stations.

Comparison of Measurement Stations: A comparison of wave heights at the ADCP station, Buoy station, and boarding point indicates that while wave height trends remain consistent under current and post-expansion conditions, slight differences exist in numerical values.

Addressing Data Gaps: Incorporating data from multiple measurement stations minimizes uncertainties caused by missing data from a single station, thereby enhancing the reliability of wave predictions and safety assessments for boarding operations.

Improved Practical Application: The findings of this study provide a more comprehensive view of wave conditions, contributing to safer and more efficient boarding operations.

Impact of Port Configuration Changes: Structural modifications, such as adding a new breakwater, influence wave patterns. These changes must be carefully evaluated to ensure the continued safety of boarding operations.

Model Accuracy and Reliability: The models used in this study demonstrate high accuracy in predicting wave conditions, confirming their practical applicability for operations at Taichung Port.
In conclusion, this study highlights the value of utilizing multiple data sources and models to improve the safety and predictability of boarding operations in challenging offshore environments. It is hoped that in the future, during the harbor expansion, similar methods can be used to analyze and evaluate possible changes in waves and further improve navigation safety.

COMPETING INTERESTS

Authors have declared that no competing interests exist.

REFERENCES

1. International Maritime Organization. Pilot Transfer Arrangements – Required Boarding Arrangements for Pilots. MSC.1/Circ.1428; 2012.
2. United States Coast Guard. Marine Safety Alert: Importance of verifying correct arrangements of handhold stanchions. Retrieved from https://www.nepia.com/uscg-issues-safety-alert-on-pilot-ladder-handhold-stanchion-arrangements/; 2022.
3. Maritime and Coastguard Agency. The code of safe working practices for merchant seamen. Retrieved from https://www.gov.uk/government/publications/code-of-safe-working-practices-for-merchant-seamen; 2015.
4. Maritime and Port Bureau, MOTC. Notice to Mariners. Retrieved from https://www.motcmpb.gov.tw; 2024.
5. Dunne G. Collisions and groundings. J Navig. 1972;25(1):113–121.
6. Wennink CJ. Collision and grounding risk analysis for ships navigating in confined waters. J Navig. 1992;45(1):80–90.
7. Hetherington C, Flin R, Mearns K. Safety in shipping: The human element. J Safety Res. 2006;37(4):401–411.
8. Montewka J, Hinz T, Kujala P, Matusiak J. Probability modelling of vessel collisions. Reliab Eng Syst Saf. 2010;95(5):573–589.
9. Schröder-Hinrichs JU. Human and organizational factors in the maritime world—Are we keeping up to speed?. WMU J Marit Aff. 2010;9(1):1–3.
10. Martins MR, Maturana MC. Application of Bayesian Belief networks to the human reliability analysis of an oil tanker operation focusing on collision accidents. Reliab Eng Syst Saf. 2013;110:89–109.
11. Uğurlu Ö, Yıldırım U, Başar E. Analysis of grounding accidents caused by human error. J Mar Sci Technol. 2015;23:748–760.
12. Mazaheri A, Montewka J, Kotilainen P, Sormunen E, Kujala P. Assessing grounding frequency using ship traffic and waterway complexity. J Navig. 2015;68(1):89–106.
13. Mazaheri A, Montewka J, Kujala P. Towards an evidence-based probabilistic risk model for ship-grounding accidents. Saf Sci. 2016;86:195–210.

14. Heij C, Knapp S. Predictive Power of Inspection Outcomes for Future Shipping Accidents–an Empirical Appraisal with Special Attention for Human Factor Aspects. Marit Policy Manag. 2018;45(5):604–621.
15. Sverdrup HU, Munk WH. Wind, Sea and Swell, Theory of Relations for Forecasting. Washington, D.C., U.S. Dept. of Navy Hydrographic Office, Pub. 601; 1947.
16. Pierson WJ, Neumann G, James RW. Practical Method for Observing and Forecasting Ocean Waves by Means of Wave Spectra and Statistics. U.S. Dept. of the Navy Hydrographic office, Pub. 603; 1955.
17. The WASA-Group. Changing waves and storms in the northeast Atlantic? Bull Am Meteorol Soc. 1998;79(5):741–760.
18. Bacon S, Carter DJT. Wave climate change in the north Atlantic and North Sea. Int J Climatol. 1991;11:545–588.
19. Bacon S, Carter DJT. A connection between mean wave height and atmospheric pressure gradient in the North Atlantic. Int J Climatol. 1993;13:423–436.
20. Sterl A, Komen G, Cotton P. Fifteen years of global wave hindcast using winds from the European Centre for Medium-Range Weather Forecast reanalysis: validation of the reanalyzed winds and assessing wave climate. J Geophys Res. 1998;103(C3):5477–5492.
21. Gulev SK, Hasse L. Changes of wind waves in the North Atlantic over the last 30 years. Int J Climatol. 1999;19:1091–1117.
22. Wang XL, Swail VR. Changes of extreme wave heights in northern hemisphere oceans and related atmospheric circulation regimes. J Clim. 2001;14:2204–2221.
23. Wang XL, Swail VR. Trends of Atlantic wave extremes as simulated in a 40-yr wave hindcast using kinematically reanalyzed wind fields. J Clim. 2002;15(9):1020–1035.
24. Cox A, Swail V. A global wave hindcast over the period 1958-1997: validation and climate assessment. J Geophys Res. 2001;106(C2):2313–2329.
25. Luo M, Shin SH. Half-century research developments in maritime accidents: Future directions. Accid Anal Prev. 2019;123:448–460.
26. Kopacz Z, Morgaś W, Urbański J. The maritime navigation an operational process, a field of study and applied science. Geodesy Cartogr. 2003;52(4).
27. Weintrit A, editor. Activities in Navigation: Marine Navigation and Safety of Sea Transportation. CRC Press; 2015.
28. Guze S, Smolarek L, Weintrit A. The area-dynamic approach to the assessment of the risks of ship collision in the restricted water. Zeszyty Naukowe Akademii Morskiej w Szczecinie. 2016;45(117):88–93.
29. Cordon JR, Mestre JM, Walliser J. Human factors in seafaring: The role of situation awareness. Saf Sci. 2017;93:256–265.
30. Durst CS. Wind speeds over short periods of time. Meteorol Mag. 1960;89:1056,181–187.
31. Taichung Port Branch. Taichung Port Vessel Traffic Service Guide. Taichung Port Branch; 2022.
32. Taichung Port Branch. Regulations for the Entry, Exit, and Berthing Operations of LNG Ships at Taichung Port. Taichung Port Branch; 2019.
33. Central Navigation Affairs Center, Maritime and Port Bureau, Ministry of Transportation and Communications. Wind Control Standards for Entry and Exit at

Taichung Port: Taichung Port Traffic Service Guide. Central Navigation Affairs Center; 2023.
34. Kirby JT. A parabolic equation for the combined refraction-diffraction of Stokes waves by mildly varying topography. J Fluid Mech. 1983;136:453–466.
35. Mizuguchi M. An heuristic model of wave height distribution in surf zone. In: Proc. 17th Coastal Eng. Conf. ASCE; 1980. p. 278–289.
36. Willmott CJ. On the validation of models. Phys Geogr. 1981;2(2):184–194.